# Tunelowanie przez nanostruktury

## Konstrukcja diagramów pasmowych

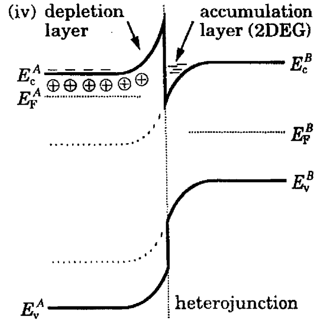


Przesuwamy tymczasowe linie $\bar{E}_c^A$ w $E_c^A$ i $\bar{E}_v^A$ w $E_v^A$, a następnie łączymy ze sobą w miejscu heterozłącza. Pojawiające się nieciągłości dopełniają szkic heterozłącza.



## Studnia trójkątna

Metoda przybliżona WKB (Wentzel – Krammers – Brillouin) – dla potencjału *wolnozmiennego*

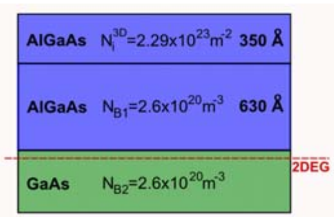


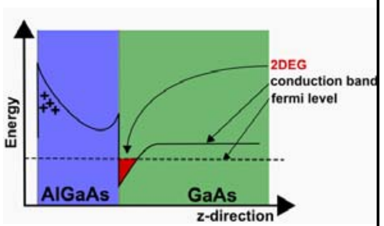


http://www.phys.unsw.edu.au/QED/research/2D_scattering.htm

$$E_n = \left[\frac{3}{2}\pi\left(n-\frac{1}{4}\right)\right]^{2/3}\left[\frac{(eF\hbar)^2}{2m}\right]^{1/3}$$

# Gęstość ładunku i prądu

Gęstość prądu: $J(\vec{r},t) = J(\vec{r}) = \frac{\hbar\, q}{2\, i\, m}(\Psi^*\nabla\Psi - \Psi\nabla\Psi^*)$

W przypadku fali de Broigla: $\Psi(x,t) = \left[A_+ e^{ikx} + A_- e^{-ikx}\right] e^{-i\omega t}$

$J(\vec{r}) = \frac{\hbar\, q\, k}{m}(|A_+|^2 - |A_-|^2)$ czyli każda fala niesie z sobą prąd

W przypadku fali zanikającej: $\Psi(x,t) = [B_+ e^{\kappa x} + B_- e^{\kappa x}] e^{-i\omega t}$

$$J(\vec{r}) = \frac{\hbar\, q\, \kappa}{i\, m}(B_+ B_-^* - B_+^* B_-) = \frac{2\, \hbar\, q\, \kappa}{m} \mathrm{Im}\,(B_+ B_-^*)$$

Tylko złożenie amplitud + i – daje rzeczywisty prąd!

Fala klasyczna: $\Psi(x,t) = Re\left\{\left[A_+ e^{ikx} + A_- e^{-ikx}\right] e^{-i\omega t}\right\}$



# Gęstość ładunku i prądu

Gęstość prądu: $J(\vec{r},t) = J(\vec{r}) = \frac{\hbar\, q}{2\, i\, m}(\Psi^*\nabla\Psi - \Psi\nabla\Psi^*)$

W przypadku fali de Broigla: $\Psi(x,t) = \left[A_+ e^{ikx} + A_- e^{-ikx}\right] e^{-i\omega t}$

$J(\vec{r}) = \frac{\hbar\, q\, k}{m}(|A_+|^2 - |A_-|^2)$ czyli każda fala niesie z sobą prąd

W przypadku fali zanikającej: $\Psi(x,t) = [B_+ e^{\kappa x} + B_- e^{\kappa x}] e^{-i\omega t}$

$$J(\vec{r}) = \frac{\hbar\, q\, \kappa}{i\, m}(B_+ B_-^* - B_+^* B_-) = \frac{2\, \hbar\, q\, \kappa}{m} \mathrm{Im}\,(B_+ B_-^*)$$

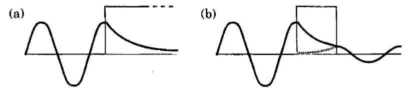


FIGURE 1.5. Current carried by counter-propagating decaying waves. (a) An infinitely thick barrier contains a single decaying exponential that carries no current. (b) A finite barrier contains both growing and decaying exponentials and passes current. (The wave function is complex, so the figure is only a rough guide.)

Tylko złożenie amplitud + i – daje rzeczywisty prąd!





# Tunelowanie

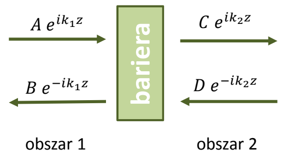


$$\begin{pmatrix} C \\ D \end{pmatrix} = T^{(21)} \begin{pmatrix} A \\ B \end{pmatrix} = \begin{pmatrix} T_{11} & T_{12} \\ T_{12}^* & T_{11}^* \end{pmatrix} \begin{pmatrix} A \\ B \end{pmatrix}$$

$$r = -\frac{T_{12}^*}{T_{11}^*} \qquad t = -\frac{1}{T_{11}^*}$$

$$T^{(21)}(0) = \begin{pmatrix} 1/t^* & -r^*/t^* \\ -r/t & 1/t \end{pmatrix}$$

Na ćwiczeniach

# Tunelowanie

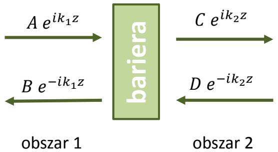


$$\begin{pmatrix} C \\ D \end{pmatrix} = T^{(21)} \begin{pmatrix} A \\ B \end{pmatrix} = \begin{pmatrix} T_{11} & T_{12} \\ T_{12}^* & T_{11}^* \end{pmatrix} \begin{pmatrix} A \\ B \end{pmatrix}$$

$$r = -\frac{T_{12}^*}{T_{11}^*} \qquad t = -\frac{1}{T_{11}^*}$$

$$T^{(21)}(0) = \begin{pmatrix} 1/t^* & -r^*/t^* \\ -r/t & 1/t \end{pmatrix}$$

$$T^{(21)}(d) = \begin{pmatrix} e^{-ik_2 d} & 0 \\ 0 & e^{ik_2 d} \end{pmatrix} T^{(21)}(0) \begin{pmatrix} e^{ik_1 d} & 0 \\ 0 & e^{ik_1 d} \end{pmatrix} = A_2^{-1}(d)\, T(0)\, A_1(d)$$

W drugą stronę: $\begin{pmatrix} B \\ A \end{pmatrix} = T^{(12)} \begin{pmatrix} D \\ C \end{pmatrix}$

$$T^{(12)}(0) = \begin{pmatrix} 1/t^* & r/t \\ r^*/t^* & 1/t \end{pmatrix}$$



# Tunelowanie

Przykłady:

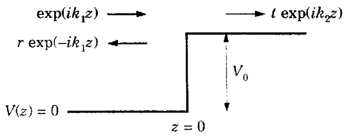


$T + R = 1$

$$T = \frac{4k_1k_2}{(k_1+k_2)^2}$$

$$R = \left(\frac{k_1-k_2}{k_1+k_2}\right)^2$$

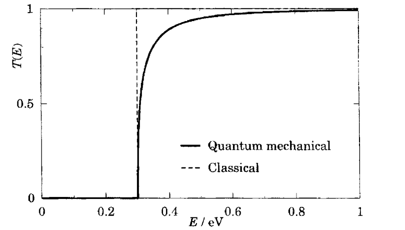


**FIGURE 5.3.** Transmission coefficient $T(E)$ as a function of the energy $E$ of the incident electron for a step 0.3 eV high in GaAs. The broken line is the classical result.



# Tunelowanie

Przykłady:

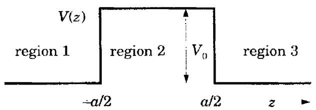


**FIGURE 5.5.** Potential barrier with $V(z) = V_0$ for $|z| < a/2$ and $V(z) = 0$ elsewhere.

Poziomy nieskończonej anty-studni!

$E > V_0$

$$T = \frac{4k_1^2k_2^2}{4k_1^2k_2^2 + (k_1^2-k_2^2)^2 \sin^2 k_2 a} = \left[1 + \frac{V_0^2}{4E(E-V_0)} \sin^2 k_2 a\right]^{-1}$$

$E < V_0$

$$T = \frac{4k_1^2\kappa_2^2}{4k_1^2\kappa_2^2 + (k_1^2+\kappa_2^2)^2 \sinh^2 \kappa_2 a} = \left[1 + \frac{V_0^2}{4E(V_0-E)} \sinh^2 \kappa_2 a\right]^{-1}$$

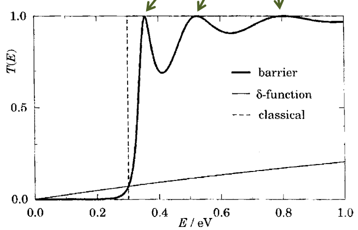


**FIGURE 5.6.** Transmission coefficient $T(E)$ as a function of energy $E$ for a square potential barrier of height $V_0 = 0.3$ eV and thickness $a = 10$ nm in GaAs. The thin curve is for a δ-function barrier of the same strength $S = V_0 a$, and the broken curve is the classical result for a barrier of the same height.



# Tunelowanie

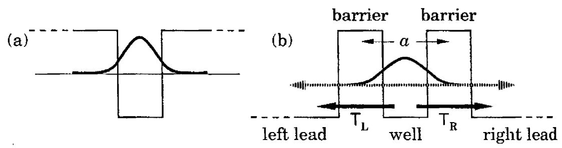


**FIGURE 5.10.** (a) A finite square potential well with a true bound state. (b) The same well but with barriers of finite thickness, where the bound state becomes resonant or quasi-bound.

$$t = \frac{t_L t_R}{1 - r_L r_R \exp 2ika}$$

$$\phi = 2ka + \rho_L + \rho_R$$

$$T = |t|^2 = \frac{T_L T_R}{\left(1-\sqrt{R_L R_R}\right)^2 + 4\sqrt{R_L R_R}\sin^2 \frac{1}{2}\phi} \qquad T_{pk} = \frac{T_L T_R}{\left(1-\sqrt{R_L R_R}\right)^2} \approx \frac{4T_L T_R}{(T_L+T_R)^2}$$

# Tunelowanie

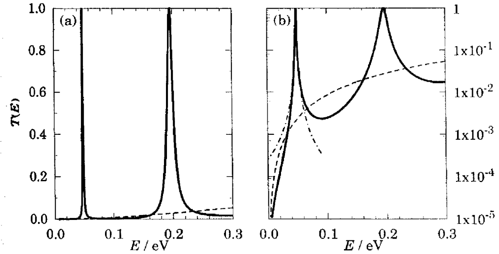


**FIGURE 5.11.** Transmission coefficient of a resonant-tunnelling structure on (a) linear and (b) logarithmic scales. The barriers are $\delta$-functions of strength 0.3 eV × 5 nm separated by 10 nm. The solid curve is $T(E)$ for the whole structure, the dashed curve shows the square of $T(E)$ for a single barrier and would apply to the double-barrier structure if there were no resonance, and the chain curve is the Lorentzian approximation to the lowest resonance.

$$T = |t|^2 = \frac{T_L T_R}{\left(1-\sqrt{R_L R_R}\right)^2 + 4\sqrt{R_L R_R}\sin^2\frac{1}{2}\phi}$$

$$T_{pk} = \frac{T_L T_R}{\left(1-\sqrt{R_L R_R}\right)^2} \approx \frac{4T_L T_R}{(T_L+T_R)^2}$$



# Tunelowanie

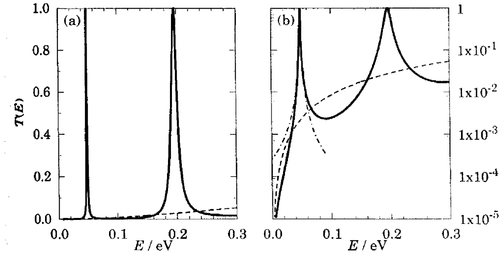


**FIGURE 5.11.** Transmission coefficient of a resonant-tunnelling structure on (a) linear and (b) logarithmic scales. The barriers are $\delta$-functions of strength 0.3 eV × 5 nm separated by 10 nm. The solid curve is $T(E)$ for the whole structure, the dashed curve shows the square of $T(E)$ for a single barrier and would apply to the double-barrier structure if there were no resonance, and the chain curve is the Lorentzian approximation to the lowest resonance.

$$T \approx \frac{T_{pk}}{1+\left(\frac{\delta\phi}{\frac{1}{2}\phi_0}\right)^2}$$

profil Lorentza

$$\phi_0 = T_L + T_R$$

$$T_{pk} = \frac{T_L T_R}{\left(1-\sqrt{R_L R_R}\right)^2} \approx \frac{4T_L T_R}{(T_L+T_R)^2}$$



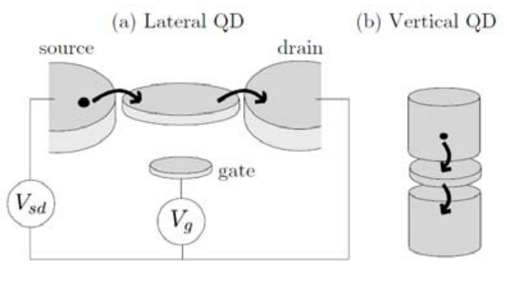


Figure 1.5: Electron flow in planar (a) and vertical (b) QD setup.



# Tunelowanie

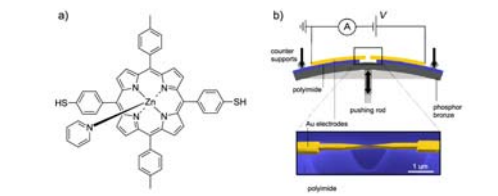


**Figure 1:** Structural formula of ZnTPPdT–Pyr (b) Top: Setup of the mechanically controllable break-junction (MCBJ). Bottom: Scanning electron micrograph of a MCBJ device (colorized for clarity). The scale bar shows that the suspended bridge is about 1 μm in length.

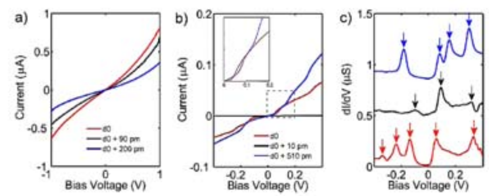


**Figure 3:** Low-temperature I(V) characteristics of junctions exposed to (a) DCM and (b) ZnTPPdT–Pyr. The DCM sample clearly shows vacuum-tunneling behavior. The porphyrin sample exhibits Coulomb blockade and steps. (c) dI/dV of a junction exposed to a ZnTPPdT–Pyr solution; curves are offset vertically for clarity. Resonances correspond to electronic or vibrational energy levels of the molecular junction. Note, for the black line the dI/dV has been scaled by a factor of 100.

## Tunelowanie

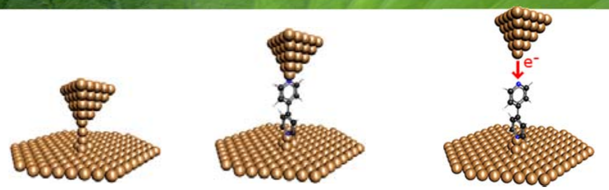


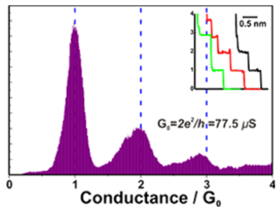


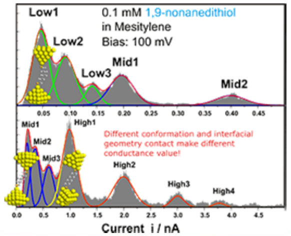


http://wandlowski.dcb.unibe.ch/research/nanostructures/me.html



## Tunelowanie

APPLIED PHYSICS LETTERS VOLUME 77, NUMBER 26 25 DECEMBER 2000

**Measurements of discrete electronic states in a gold nanoparticle using tunnel junctions formed from self-assembled monolayers**

Jason R. Petta,[a] D. G. Salinas, and D. C. Ralph
Laboratory of Atomic and Solid State Physics, Cornell Univer

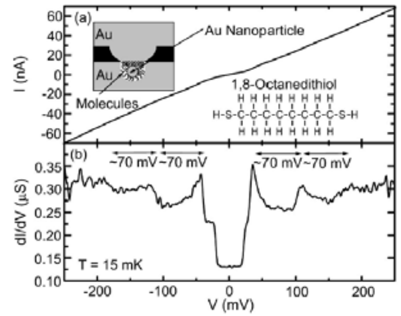


FIG. 2. (a) $I$–$V$ curve for a device containing an Au nanoparticle wi 1,8-octanedithiol barriers. (b) $dI/dV$–$V$ determined by numerical differe tiation. The regularly spaced peaks in $dI/dV$ indicate tunneling though single particle. Inset: Device schematic.



## Tunelowanie

TOPICAL REVIEW

**Effects of electron–vibration coupling in transport through single molecules**

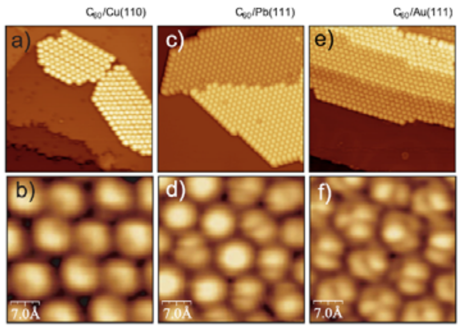


**Figure 2.** Large scale STM images and zoomed regions enhancing the intramolecular resolution of $C_{60}$ monolayer islands grown on ((a), (b)) Cu(110), ((c), (d)) Pb(111) and ((e), (f)) Au(111). In all cases, the STM images were obtained with positive sample bias, hence corresponding to the unoccupied density of states. In this way, the lobed structure observed in some molecules can be identified with the spatial shape of unoccupied orbitals. Reproduced with permission from [108]. Copyright 2011 Pan Stanford Publishing.



## Tunelowanie

TOPICAL REVIEW

**Effects of electron–vibration coupling in transport through single molecules**

Katharina J Franke and Jose Ignacio Pascual
Fachbereich Physik, Freie Universität Berlin, Arnimallee 14, 14195 Berlin, Germany

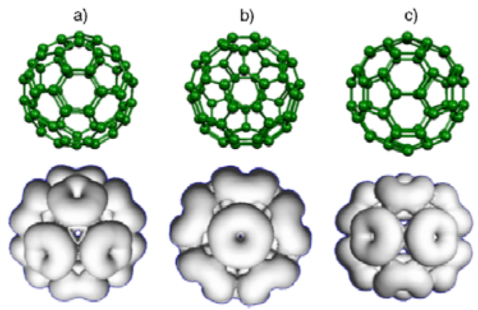


**Figure 1.** Molecular structure of a $C_{60}$ molecule. When the molecule is adsorbed on a surface, there are three outstanding high-symmetry orientations. The molecule may expose (a) a hexagon on top, (b) a pentagon on top, or (c) a C–C double bond on top. The LUMO isosurface is mainly located on the carbon pentagons, giving rise to the typical symmetries seen in STM images for the three orientations (compare figure 2).

# Tu

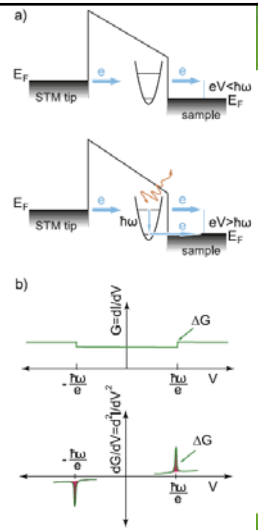


TOPICAL REVIEW

**Effects of electron–vibration coupling in transport through single molecules**

Katharina J Franke and Jose Ignacio Pascual

**Figure 4.** (a) Model potential tunneling barrier with a molecule placed in the barrier. The molecular vibrations are represented as a simple harmonic oscillator. When the energy of the tunneling electrons is below any molecular excitation they can only tunnel elastically. When the electron energy exceeds the energy threshold for molecular excitation an additional tunneling path is opened, where the electrons tunnel inelastically off the molecule. (b) The effect of the inelastic channels is ideally a small step-wise increase in the differential tunneling conductance ($dI/dV$–$V$). This induces a peak in the $d^2I/dV^2$–$V$ spectrum.



# Tunelowanie

TOPICAL REVIEW

**Effects of electron–vibration coupling in transport through single molecules**

Katharina J Franke and Jose Ignacio Pascual

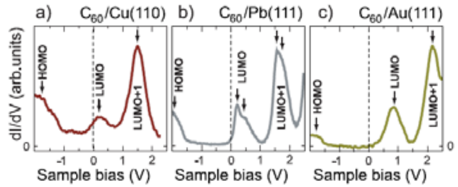


**Figure 3.** Differential conductance spectra of $C_{60}$ on the different surfaces shown in figure 2. Arrows mark the fitted positions of HOMO, LUMO and LUMO + 1. The spectra were measured by positioning the STM tip on top of a single molecule and ramping the bias voltage $V$ while keeping the tip–molecule distance constant (feedback loop open). Arrows identify the molecular states. $dI/dV$ data were obtained by using a lock-in amplifier with an rms modulation amplitude $V_{ac}$. (Cu: $R_{junct} = 1.1$ GΩ, $V_{ac} = 20$ mV; Pb: $R_{junct} = 0.7$ GΩ, $V_{ac} = 5$ mV; Au: $R_{junct} = 0.3$ GΩ, $V_{ac} = 30$ mV.) Reproduced with permission from [108]. Copyright 2011 Pan Stanford Publishing.



# Tunelowanie

Science AAAS

**Conductance of a Molecular Junction**
M. A. Reed *et al.*
*Science* **278**, 252 (1997);
DOI: 10.1126/science.278.5336.252

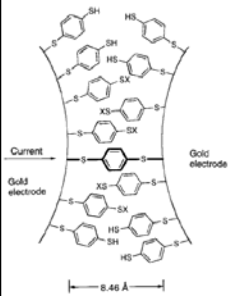


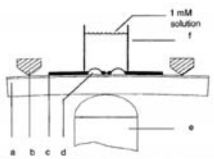


**Fig. 1.** A schematic of the MCB junction with (a) the bending beam, (b) the counter supports, (c) the notched gold wire, (d) the glue contacts, (e) the piezo element, and (f) the glass tube containing the solution.

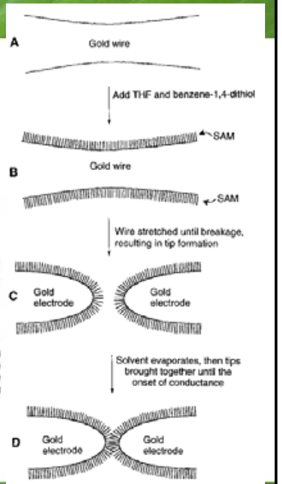




# Tunelowanie

Science AAAS

**Conductance of a Molecular Junction**
M. A. Reed *et al.*
*Science* **278**, 252 (1997);

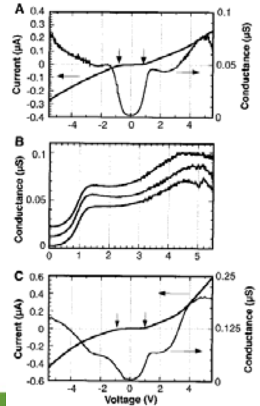


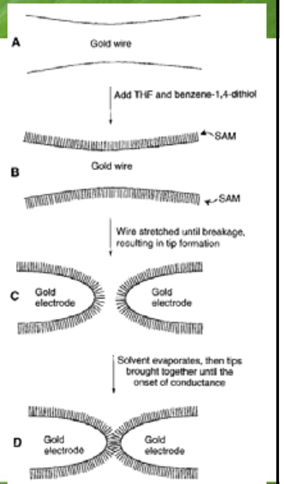

# State-of-the-Art: Electronic Circuits

Kees Hummelen - University of Groningen

From macroscopic copper (~ 1 μm) to nanoscale electronics organic molecules (~0.3- 3 nm)

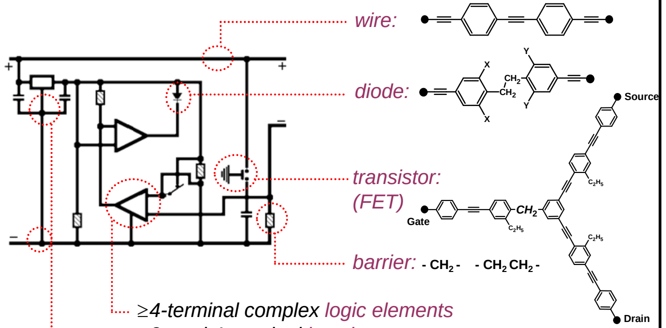


Jaszowiec 0606'05

2013-02-27 25

# Nanoprzełączniki

**Self-assembled monolayer organic field-effect transistors**

Jan Hendrik Schön, Hong Meng & Zhenan Bao

*Bell Laboratories, Lucent Technologies, Mountain Avenue, Murray Hill, New Jersey 07974, USA*

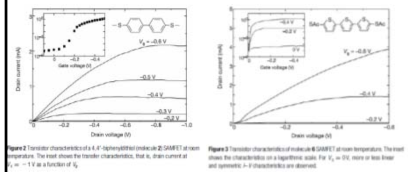

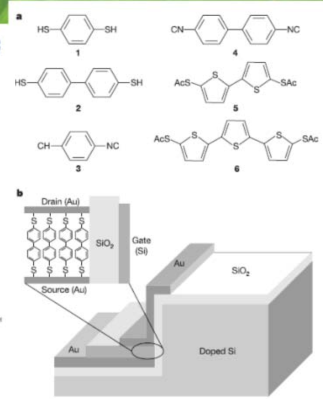


**Figure 1** Structure of the investigated molecules and transistors. **a**, Molecular structure of the investigated materials; **b**, SAMFET structure: a highly doped Si-substrate is used as the gate electrode, a thermally grown SiO2 layer acts as gate insulator, the gold source electrode is deposited by thermal evaporation, the active semiconducting material is a self-assembled monolayer (SAM) of one of the six molecules (1–6), and the drain contact is defined by shallow-angle shadow evaporation of gold. The active region of the device is magnified.

2013-02-27

# Nanoprzełączniki

**REPORT OF THE INVESTIGATION COMMITTEE ON THE POSSIBILITY OF SCIENTIFIC MISCONDUCT IN THE WORK OF HENDRIK SCHÖN AND COAUTHORS**

http://www.lucent.com/news_events/pdf/researchreview.pdf

September 2002

**Self-assembled monolayer organic field-effect transistors**

Jan Hendrik Schön, Hong Meng & Zhenan Bao

*Nature* 413, 713–716 (2001); correction *Nature* 414, 470 (2001).

This manuscript was, in part, the subject of an independent investigation[1] conducted at the behest of Bell Laboratories, Lucent Technologies. The independent committee reviewed concerns related to the validity of data associated with the device measurements described in the paper. As a result of the committee's findings, we are issuing a retraction of the paper. We note nevertheless that this paper may also contain some legitimate ideas and contributions. □

1. Beasley, M. R., Datta, S., Kogelnik, H., Kroemer, H. & Monroe, D. Report of the Investigation Committee on the Possibility of Scientific Misconduct in the Work of Hendrik Schön and Coauthors. (http://publish.aps.org/reports/) (doi:10.1103/aps.reports.lucent) (Lucent Technologies/American Physical Society, September 2002).

*Figure 3. Original plotting data from Figure 1 and Figure 2 (extracted from an electronic draft), replotted to illustrate that the data present in both are* **exactly** *the same, after dividing the latter by 2. All but a few of the solid symbols are within the open symbols, and agree with each other to five significant figures, although they represent distinct data sets.*

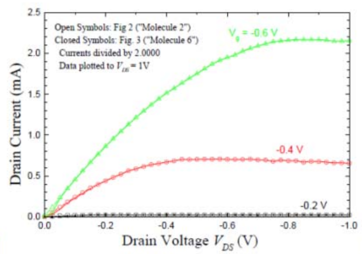


2013-02-27 27

# State-of-the-Art: Electronic Circuits

Kees Hummelen - University of Groningen

From macroscopic copper (~ 1 μm) to nanoscale electronics organic molecules (~0.3- 3 nm)

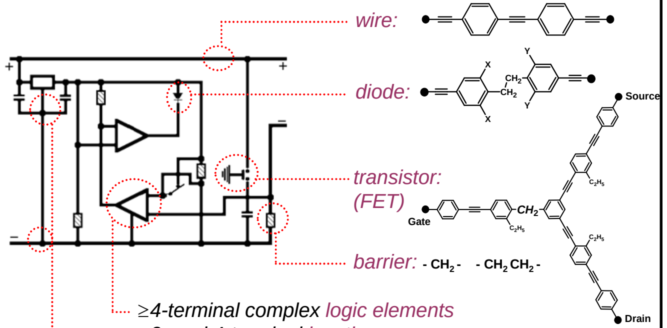


Jaszowiec 0606'05

2013-02-27 28

## State-of-the-Art: Electronic Circuits

Kees Hummelen - University of Groningen

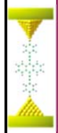

3-terminal junctions: 'Tour' wires[1]

*M.A. Ratner et. al.*[2]

*"…failure to measure transport when built on meta-positions…"*

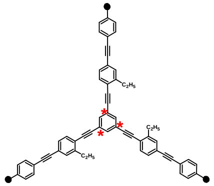

≥4-terminal: junctions … no examples

logic elements, AND-gate:

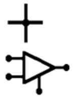

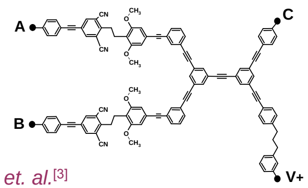


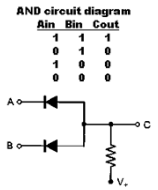


*C. Joachim et. al.*[3]

*"…molecules remain based on 3-branch molecules…"*

[3] *Chem. Phys. Lett.*, 2003, 367, 662.



[1] *J.Am.Chem.Soc.*, 1998, 120, 8486. [2] *Ann. NY. Acad. Sci.*, 2002, 960, 153.



## Hwang Woo-Suk

SCIENCE VOL 308 17 JUNE 2005

### Patient-Specific Embryonic Stem Cells Derived from Human SCNT Blastocysts

Woo Suk Hwang,[1,2*] Sung Il Roh,[3] Byeong Chun Lee,[1] Sung Keun Kang,[1] Dae Kee Kwon,[1] Sue Kim,[1] Sun Jong Kim,[3] Sun Woo Park,[1] Hee Sun Kwon,[1] Chang Kyu Lee,[2] Jung Bok Lee,[3] Jin Mee Kim,[3] Curie Ahn,[4] Sun Ha Paek,[4] Sang Sik Chang,[5] Jung Jin Koo,[5] Hyun Soo Yoon,[6] Jung Hye Hwang,[6] Youn Young Hwang,[6] Ye Soo Park,[6] Sun Kyung Oh,[4] Hee Sun Kim,[4] Jong Hyuk Park,[7] Shin Yong Moon,[4] Gerald Schatten[7*]

Patient-specific, immune-matched human embryonic stem cells (hESCs) are anticipated to be of great biomedical importance for studies of disease and development and to advance clinical deliberations regarding stem cell transplantation. Eleven hESC lines were established by somatic cell nuclear transfer (SCNT) of skin cells from patients with disease or injury into donated oocytes. These lines, nuclear transfer (NT)–hESCs, grown on human feeders from the same NT donor or from genetically unrelated individuals, were established at high rates, regardless of NT donor sex or age. NT-hESCs were pluripotent, chromosomally normal, and matched the NT patient's DNA. The major histocompatibility complex identity of each NT-hESC when compared to the patient's own showed immunological compatibility, which is important for eventual transplantation. With the generation of these NT-hESCs, evaluations of genetic and epigenetic stability can be made. Additional work remains to be done regarding the development of reliable directed differentiation and the elimination of remaining animal components. Before clinical use of these cells can occur, preclinical evidence is required to prove that transplantation of differentiated NT-hESCs can be safe, effective, and tolerated.

Hwang Woo-Suk



## Hwang Woo-Suk

### RETRACTION

*Post date 12 January 2006*

The final report from the Investigation Committee of Seoul National University (SNU) (*1*) has concluded that the authors of two papers published in *Science* (*2, 3*) have engaged in research misconduct and that the papers contain fabricated data. With regard to Hwang *et al.*, 2004 (*2*), the Investigation Committee reported that the data showing that DNA from human embryonic stem cell line NT-1 is identical to that of the donor are invalid because they are the result of fabrication, as is the evidence that NT-1 is a bona fide stem cell line. Further, the committee found that the claim in Hwang *et al.*, 2005 (*3*) that 11 patient-specific embryonic stem cells line were derived from cloned blastocysts is based on fabricated data. According to the report of the Investigation Committee, the laboratory "does not possess patient-specific stem cell lines or any scientific basis for claiming to have created one." Because the final report of the SNU investigation indicated that a significant amount of the data presented in both papers is fabricated, the editors of *Science* feel that an immediate and unconditional retraction of both papers is needed. We therefore retract these two papers and advise the scientific community that the results reported in them are deemed to be invalid.

As we post this retraction, seven of the 15 authors of Hwang *et al.*, 2004 (*2*) have agreed to retract their paper. All of the authors of Hwang *et al.*, 2005 (*3*) have agreed to retract their paper.

*Science* regrets the time that the peer reviewers and others spent evaluating these papers as well as the time and resources that the scientific community may have spent trying to replicate these results.

**Donald Kennedy**
Editor-in-Chief



## Hwang Woo-Suk

Hwang Woo-Suk

SCIENCE VOL 303 12 MARCH 2004

### Evidence of a Pluripotent Human Embryonic Stem Cell Line Derived from a Cloned Blastocyst

Woo Suk Hwang,[1,2*] Young June Ryu,[1] Jong Hyuk Park,[3] Eul Soon Park,[1] Eu Gene Lee,[1] Ja Min Koo,[4] Hyun Yong Jeon,[1] Byeong Chun … hn,[5] Jung H…

Somatic cell nucle… erate animals with a co… vation of a pluripotent e… uman blastocyst. The SC… rface markers and were… nd of forming teratomas… germ layers in severe co… n for more than 70 pas… were genetically identic… letely exclude the possibility that the cells had a parthenogenetic origin, imprinting analyses support a SCNT origin of the derived human ES cells.

## Kwant przewodnictwa

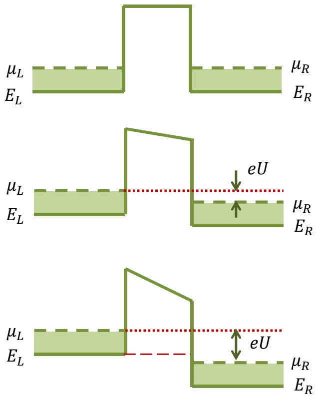


$$I = I_L + I_R$$

$$I_L = \frac{2e}{h}\int_{E_L}^{\infty} f(E,\mu_L)T(E)dE$$

$$I_R = -\frac{2e}{h}\int_{E_R}^{\infty} f(E,\mu_R)T(E)dE$$

$$I = \frac{2e}{h}\int_{E_L}^{\infty} [f(E,\mu_L) - f(E,\mu_R)]T(E)dE$$

**Na ćwiczeniach**

$$I = \frac{2e}{h}\int_{E_L}^{\infty} f(E,\mu_L)T(E)dE$$



## Kwant przewodnictwa

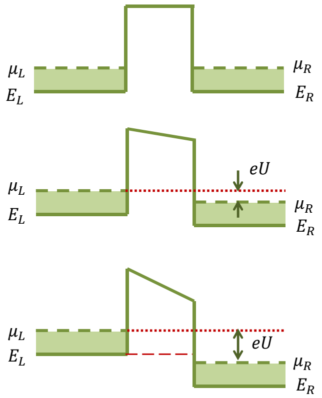


Dla temperatury $T \to 0$:

$$I = \frac{2e}{h}\int_{\mu_R}^{\mu_L} [f(E,\mu_L) - f(E,\mu_R)]T(E)dE$$

$$I = \frac{2e}{h}\int_{E_L}^{\mu_L} f(E,\mu_L)T(E)dE$$



## Kwant przewodnictwa

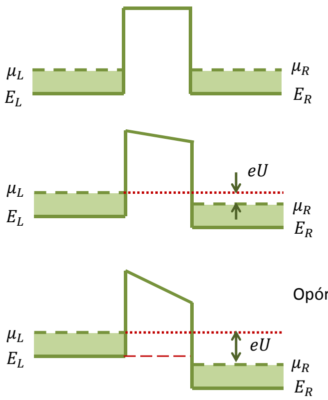


Dla metali $\mu_L = \mu + \frac{1}{2}eU$ i $\mu_R = \mu - \frac{1}{2}eU$ :

$$f(E,\mu_L) - f(E,\mu_R) \approx$$
$$\approx eU\frac{\partial f(E,\mu)}{\partial \mu} = -eU\frac{\partial f(E,\mu)}{\partial E}$$

$$I = \frac{2e^2U}{h}\int_{E_L}^{\infty} \frac{\partial f(E,\mu)}{\partial E}T(E)dE \approx$$

$$G = \frac{dI}{dU} = \frac{2e^2}{h}\int_{E_L}^{\infty} \frac{\partial f(E,\mu)}{\partial E}T(E)dE \approx \frac{2e^2}{h}T(\mu)$$

Opór jest skończony nawet dla idealnego przewodnika!

$$\frac{e^2}{h} = 38{,}7\ \mu S \qquad \frac{h}{e^2} = 25{,}8\ k\Omega$$

Kwant przewodnictwa (w simensach)



## Kwant przewodnictwa

$$G = \frac{dI}{dU} = \frac{2e^2}{h}\int_{E_L}^{\infty} \frac{\partial f(E,\mu)}{\partial E}T(E)dE \approx \frac{2e^2}{h}T(\mu) = 2G_0T(\mu)$$

$$\frac{e^2}{h} = 38{,}7\ \mu S$$

Wzór Landauera (*Landauer formula*) – gdy mamy do czynienia z wieloma kanałami przewodnictwa

$$G = G_0\sum_n T_n(\mu) \approx NG_0$$

$N$ to suma różnych „pełnych" kanałów przewodnictwa np. dwa różne spiny dają $N = 2$

Dla $T = const$ dostajemy prawo Ohma.

# Studnia trójkątna

Metoda przybliżona WKB (Wentzel – Krammers – Brillouin) – dla potencjału *wolnozmiennego*

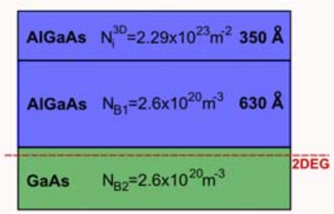


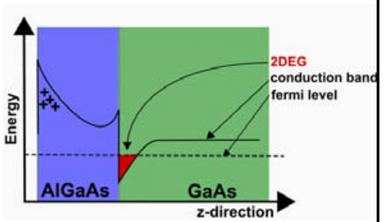


http://www.phys.unsw.edu.au/QED/research/2D_scattering.htm

$$E_n = \left[\frac{3}{2}\pi\left(n-\frac{1}{4}\right)\right]^{2/3}\left[\frac{(eF\hbar)^2}{2m}\right]^{1/3}$$



# Studnia trójkątna

Metoda przybliżona WKB (Wentzel – Krammers – Brillouin) – dla potencjału *wolnozmiennego*

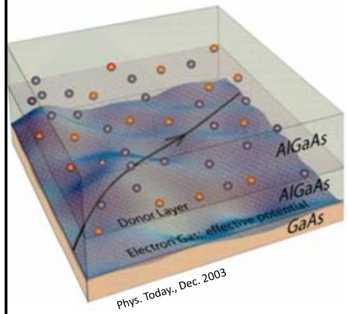


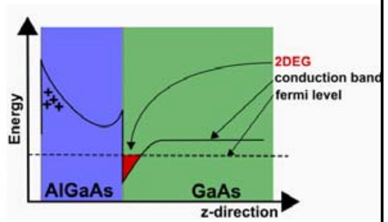


http://www.phys.unsw.edu.au/QED/research/2D_scattering.htm

$$E_n = \left[\frac{3}{2}\pi\left(n-\frac{1}{4}\right)\right]^{2/3}\left[\frac{(eF\hbar)^2}{2m}\right]^{1/3}$$



# Kwant przewodnictwa

$$G = \frac{dI}{dU} = \frac{2e^2}{h}\int_{E_L}^{\infty}\frac{\partial f(E,\mu)}{\partial E}T(E)dE \approx \frac{2e^2}{h}T(\mu) = G_0 T(\mu)$$

$$\frac{e^2}{h} = 38{,}7\ \mu S$$

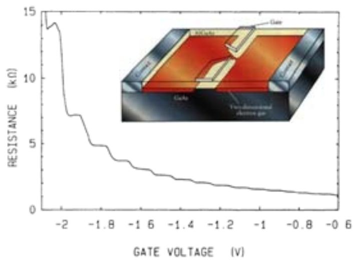


FIG. 1. Point-contact resistance as a function of gate voltage at 0.6 K. Inset: Point-contact layout.

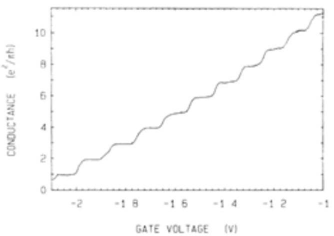


FIG. 2. Point-contact conductance as a function of gate voltage, obtained from the data of Fig. 1 after subtraction of the lead resistance. The conductance shows plateaus at multiples of $e^2/\pi\hbar$.

B. J. van Wees et al. *Quantized conductance of point contacts in a two-dimensional electron gas* Phys. Rev. Lett. **60**, 848–850 (1988)



# Kwant przewodnictwa

$$G = \frac{2e^2}{h}T(\mu) = G_0 T(\mu)$$

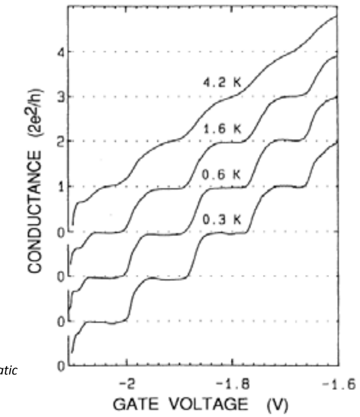


B. J. van Wees et al. *Quantum ballistic and adiabatic electron transport studied with quantum point contacts* Phys. Rev. B 43, 12431–12453 (1991)

FIG. 6. Breakdown of the conductance quantization due to temperature averaging. The curves have been offset for clarity.

# Kwant przewodnictwa

$$G = \frac{2e^2}{h}T(\mu) = G_0 T(\mu)$$

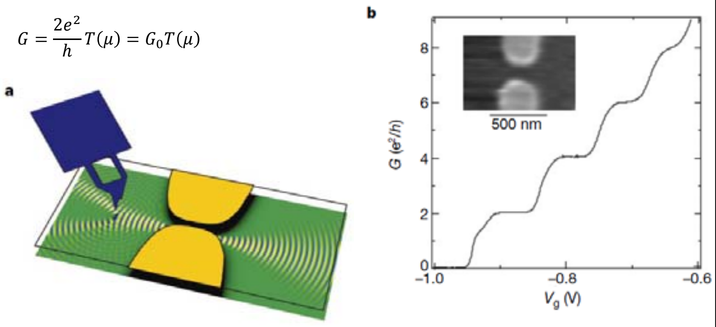


M. A. Topinka et al. *Coherent branched flow in a two-dimensional electron gas* Nature 410, 183 (2001)



# Kwant przewodnictwa

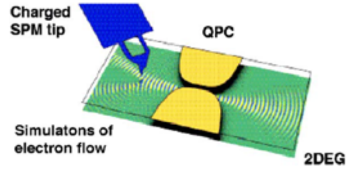


Fig. 1. Schematic diagram showing a negatively charged SPM tip positioned above a quantum point contact (QPC) formed in a two-dimensional electron gas (2DEG) by electrostatic gates. Simulations of electron flow in the diagram show how electron waves are scattered by the depleted disc beneath the tip Topinka et al. [16].

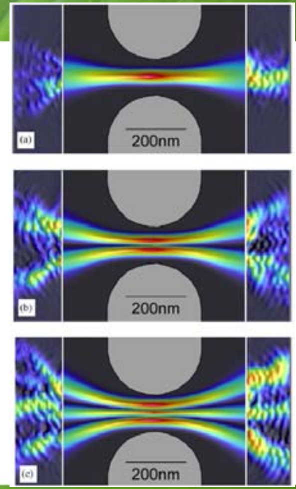


Fig. 2. Experimental images (outside) and theoretical simulations (inside) of the flow of electron waves through a quantum point contact for the first three modes (a)–(c). Fringes spaced by half the Fermi wavelength demonstrate coherence in the flow Topinka et al. [6].

R.M. Westervelt, M. A. Topinka et al. Physica E 24 (2004) 63–69



# Kwant przewodnictwa

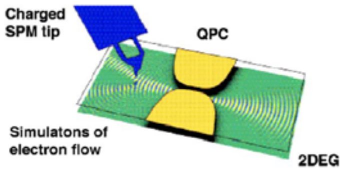


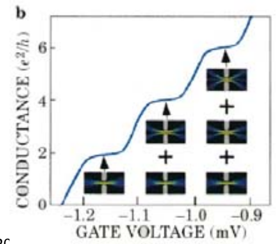


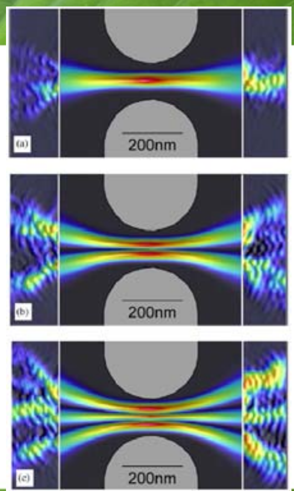


Physica E 24 (2C



# Kwant przewodnictwa

$$G = \frac{2e^2}{h}T(\mu) = G_0 T(\mu)$$

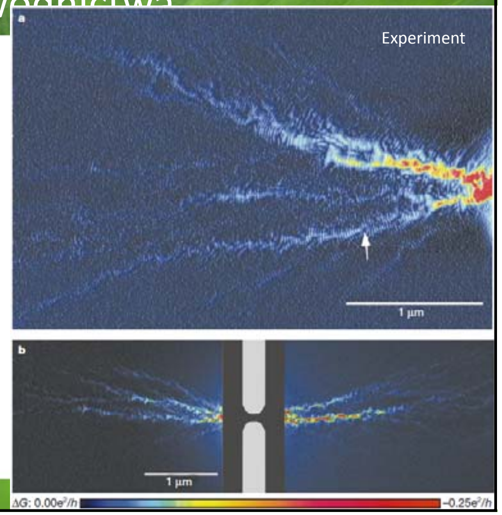


M. A. Topinka et al. Nature 410, 183 (2001)

## Kwant przewodnictwa

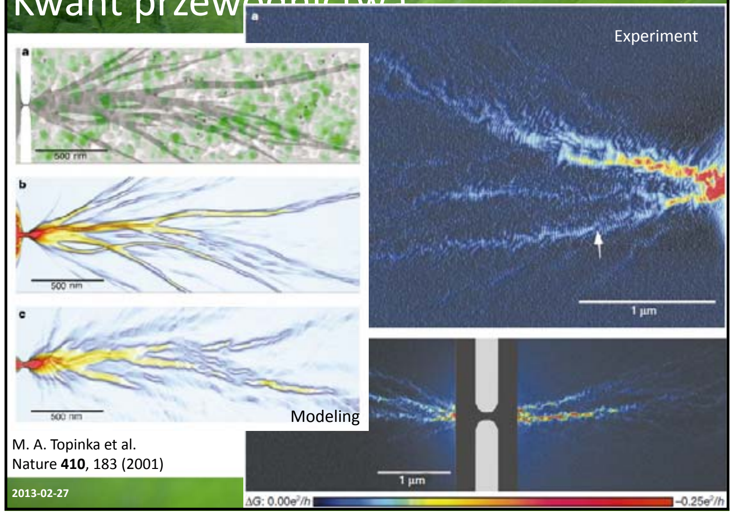


M. A. Topinka et al.
Nature **410**, 183 (2001)



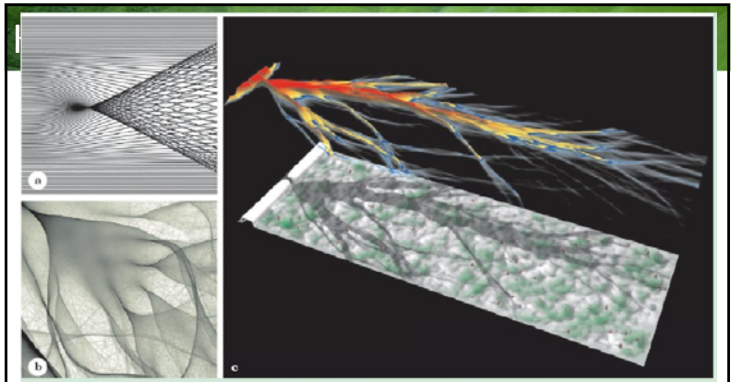

**Figure 6. Simulations of electron flow. (a)** Parallel electron trajectories, going from left to right, form a V-shaped cusp due to focusing by a potential-energy dip caused by a charged donor atom (not seen) above a two-dimensional electron gas. **(b)** A realistic 2DEG simulation that includes many ionized donors forms several generations of cusps. The electrons travel here from upper left to lower right. **(c)** Ray-tracing simulations of electron flux emerging from a small opening into a region of random potential reflect the features seen in experimental images of 2DEG quantum point contact samples. The potential is shown green in the valleys and white on the peaks. The electron flux is coded by height and color, with blue corresponding to regions of low flux; still lower flux is transparent. The "shadow" of the flux on the potential plot shows where the flux lies relative to the hills and valleys; no guiding valleys are seen. A slight change of the position of the opening changes the location and direction of the branches. (S. E. J. Shaw, PhD thesis, Harvard University, 2002.)



## Kwant przewodnictwa

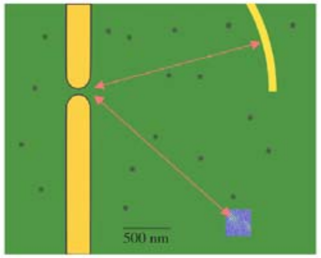


Fig. 3. Schematic diagram showing how a V-shaped electron interferometer was constructed using a QPC and a reflecting gate (gates in gold color). The SPM tip was scanned over the small blue area at approximately the same distance from the QPC as the reflector gate. Electrons passing from the QPC travel along both legs of the interferometer at once (paths shown in red, with arrows), and interfere when they return to their starting point.

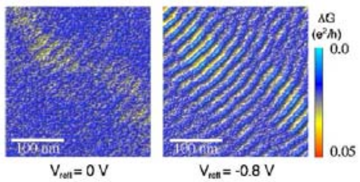


Fig. 4. Experimental images that show that fringes are created in the interferometer of Fig. 3, when the reflector mirror is turned on by depleting the electron gas below. Only weak fringes are observed in the left panel when the reflector mirror is off ($V_{refl} = 0$ V), while strong fringes are observed in the right panel when the reflector mirror is on ($V_{refl} = -0.8$ V).

R.M. Westervelt, M. A. Topinka et al.
Physica E 24 (2004) 63–69



## Kwant przewodnictwa

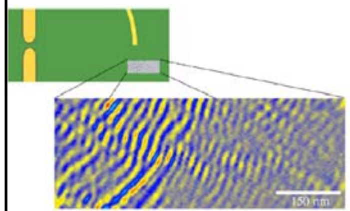


Fig. 6. Image of fringes in an electron interferometer that show how the fringe intensity varies with distance from the QPC—the fringes are strongest at the same distance from the QPC as the reflector mirror. An ensemble average over the thermal distribution of electron energies tends to wash out fringes at other distances.

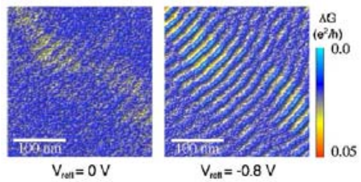


Fig. 4. Experimental images that show that fringes are created in the interferometer of Fig. 3, when the reflector mirror is turned on by depleting the electron gas below. Only weak fringes are observed in the left panel when the reflector mirror is off ($V_{refl} = 0$ V), while strong fringes are observed in the right panel when the reflector mirror is on ($V_{refl} = -0.8$ V).

R.M. Westervelt, M. A. Topinka et al.
Physica E 24 (2004) 63–69

# Tunelowanie

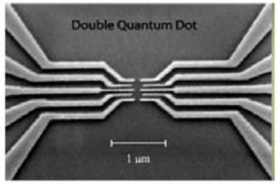


Jeong, Chang, Melloch *Science* **293** 2222 (2001)

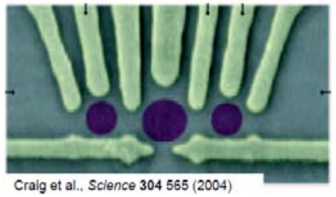

Craig et al., *Science* **304** 565 (2004)

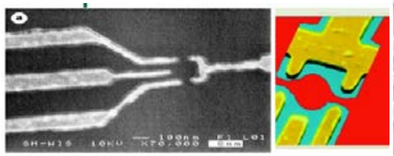

Goldhaber-Gordon *et al.* *Nature* **391** 156 (1998)

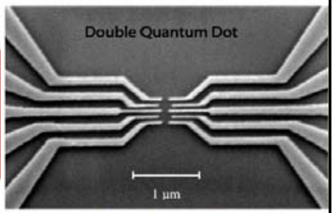


Jeong, Chang, Melloch *Science* **293** 2222 (2001)



# Tunelowanie

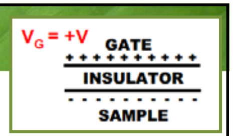


Kropka zachowuje się jak mały kondensator o energii $E_c \sim \frac{1}{2}\frac{e^2}{C}$

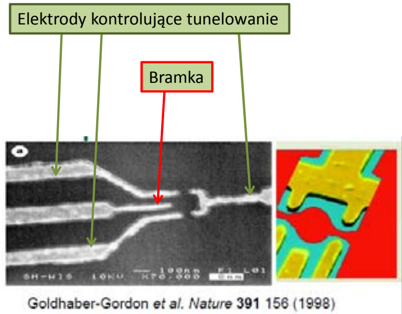


Goldhaber-Gordon *et al.* *Nature* **391** 156 (1998)

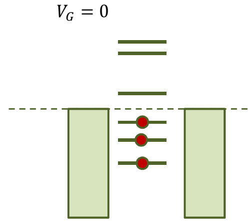




# Blokada Kulombowska

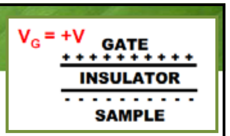


Kropka zachowuje się jak mały kondensator o energii $E_c \sim \frac{1}{2}\frac{e^2}{C}$

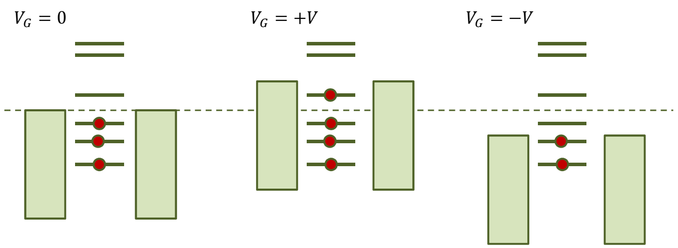




# Blokada Kulombowska

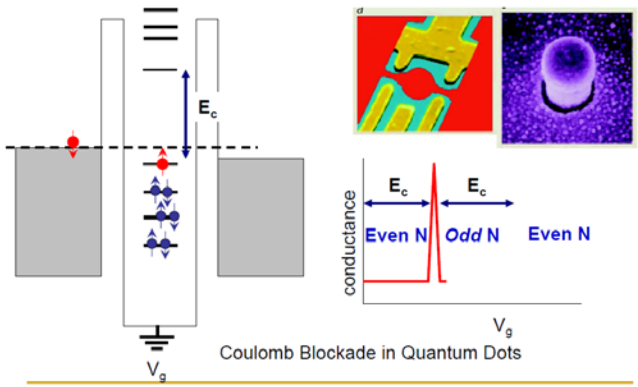


Y. Alhassid *Rev. Mod. Phys.* **72** 895 (2000).

http://sces.phys.utk.edu/~dagotto/condensed/Lectures_2008/UTK_Lecture1_March08.pdf

Luis Dias – UT/ORNL

# Blokada Kulombowska

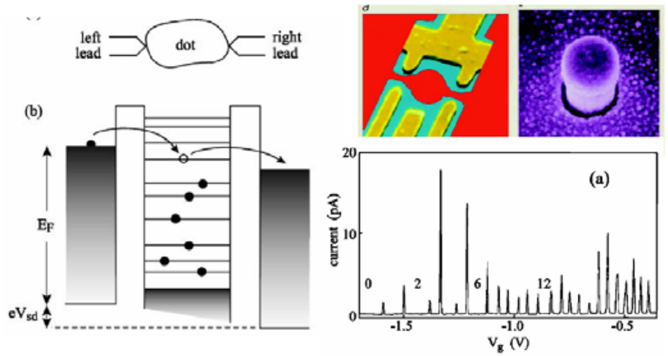


Coulomb Blockade in Quantum Dots: “dot spectroscopy”

http://sces.phys.utk.edu/~dagotto/condensed/Lectures_2008/UTK_Lecture1_March08.pdf

Luis Dias – UT/ORNL



# Blokada Kulombowska

Kropka zachowuje się jak mały kondensator o energii $E_c \sim \frac{1}{2}\frac{e^2}{C}$

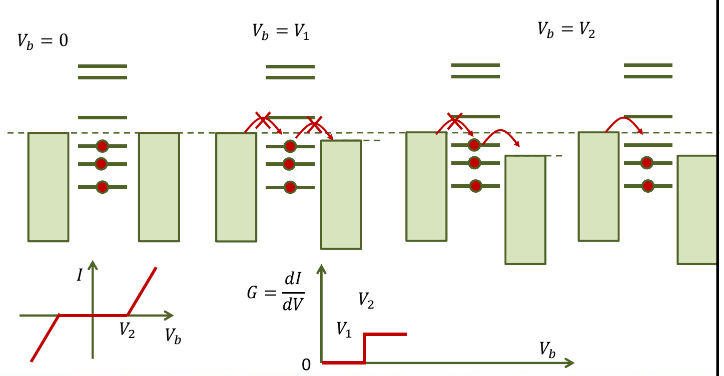




# Blokada Kulombowska

Kropka zachowuje się jak mały kondensator o energii $E_c \sim \frac{1}{2}\frac{e^2}{C}$

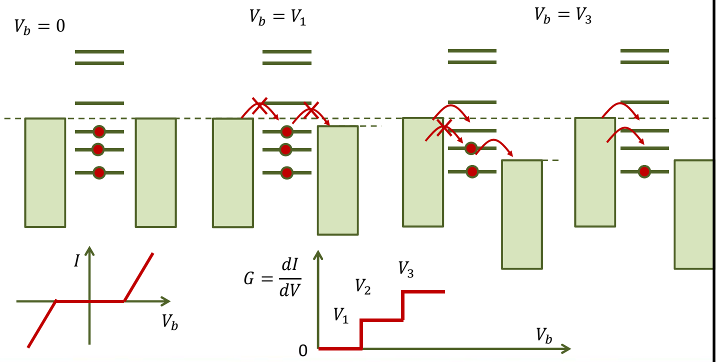




# Blokada Kulombowska

Kropka zachowuje się jak mały kondensator o energii $E_c \sim \frac{1}{2}\frac{e^2}{C}$

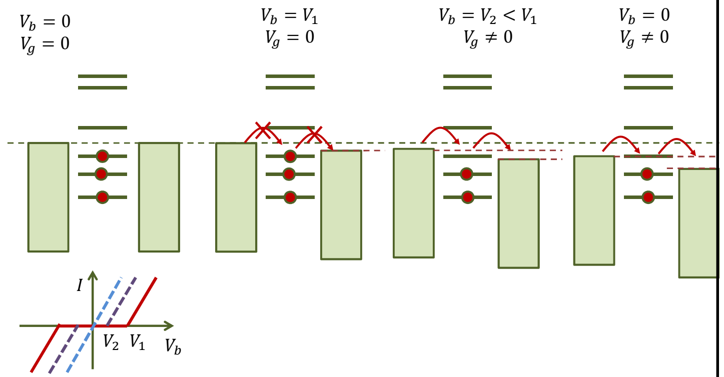

## Blokada Kulombowska

Kropka zachowuje się jak mały kondensator o energii $E_c \sim \frac{1}{2}\frac{e^2}{C}$

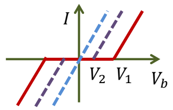


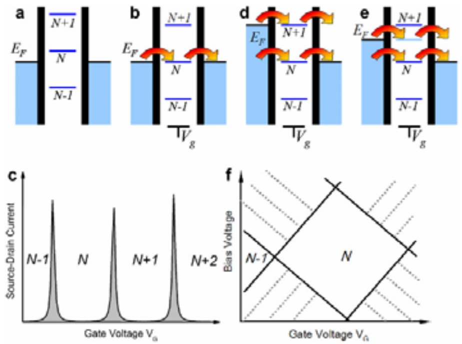


Inorganica Chimica Acta 361 (2008) 3807–3819



## Blokada Kulombowska

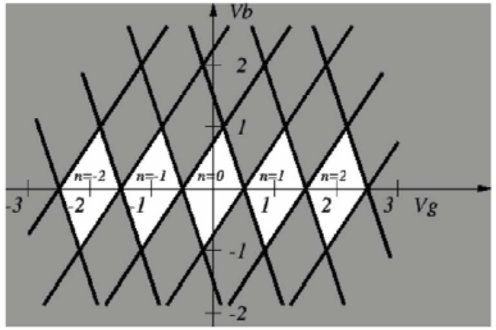


**Figure 6:** “Coulomb diamonds”

http://www.dstuns.iitm.ac.in/teaching-and-presentations/teaching/undergraduate%20courses/vy305-molecular-architecture-and-evolution-of-functions/presentations/presentations-2007/seminar-2/P2.pdf



## Blokada Kulombowska

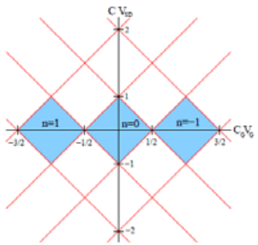


Figure 6.6: A stability diagram for a SET. The blue shaded regions are the Coulomb diamonds, where the number of electrons on the dot is fixed at $n$ and transport through the dot is blocked. Red lines indicate voltages where the number of addition energies within the transport window changes by one. We have set $e = 1$ here for convenience.

Clive Emary
Theory of Nanostructures nanoskript.pdf



## Blokada Kulombowska

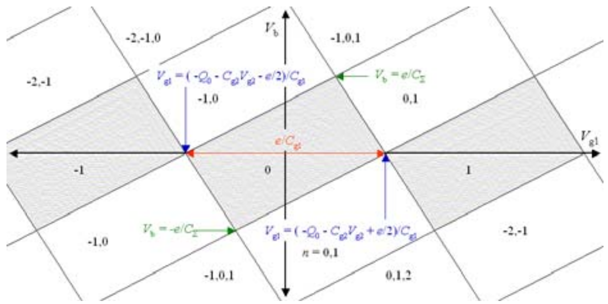


http://lamp.tu-graz.ac.at/~hadley/ss2/set/transistor/coulombblockade.php

# Blokada Kulombowska

**Excitation Spectra of Circular, Few-Electron Quantum Dots**

L. P. Kouwenhoven, T. H. Oosterkamp, M. W. S. Danoesastro, M. Eto, D. G. Austing, T. Honda, S. Tarucha

SCIENCE • VOL. 278 • 5 DECEMBER 1997

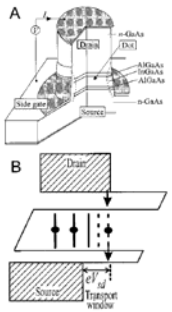


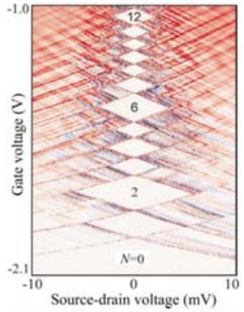


**Fig. 2.** Differential conductance $\partial I/\partial V_{sd}$ plotted in color scale in the $V_g - V_{sd}$ plane at $B = 0$. In the white diamond-shaped regions, $\partial I/\partial V_{sd} \approx 0$ as a result of Coulomb blockade. $N$ is fixed in each of the diamond regions. The lines outside the diamonds, running parallel to the sides, identify excited states.



# Blokada Kulombowska

Figure 6.7: The low temperature conductances of (a) a metal single-electron transistor (SET), (b) a semiconducting SET, (c) a carbon nanotube SET, and (d) a superconducting SET are plotted as a function of gate voltage and bias voltage. The diamond shaped regions along the zero bias voltage axis are regions of Coulomb blockade. The conductance is a periodic function of gate voltage for the metal SET and the superconducting SET where the confinement energy is negligible. The conductance is not a periodic function of gate voltage for the semiconductor SET and the carbon nanotube SET where the confinement energy is important. From: P. Hadley and J.E. Mooij, Delft University of Technology, http://qt.tn.tudelft.nl/publi/2000/quantumdev/qdevices.html

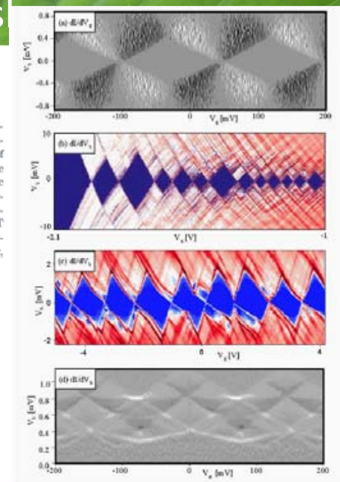

Clive Emary
Theory of Nanostructures nanoskript.pdf



# Blokada Kulombowska

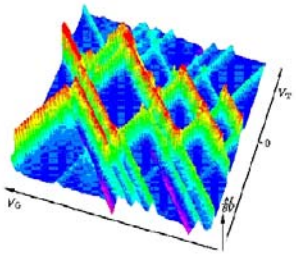

Dodatkowe „diamenty" – np. efekty spinowe , stany wzbudzone itp

http://www-ipcms.u-strasbg.fr/spip.php?article491&lang=en

*Figure 1 :* The differential conductance, calculated in the regime of sequential tunneling through a one-dimensional quantum dot, as a function of the gate voltage (to the left) and the transport voltage. Green and red: Positive values. Blue: Close to zero. Pink: Negative differential conductance. The Coulomb blockade diamonds are aligned along the gate voltage axis. In parallel, one observes structures which are due to excited states of the dot. Electronic correlations combined with spin selection rules lead to the regions of negative differential conductance.



# Blokada Kulombowska

nature physics LETTERS
PUBLISHED ONLINE: 6 APRIL 2009 | DOI: 10.1038/NPHYS1234

**Franck-Condon blockade in suspended carbon nanotube quantum dots**

Renaud Leturcq[1,2*], Christoph Stampfer[1,3*], Kevin Inderbitzin[1], Lukas Durrer[3], Christofer Hierold[3], Eros Mariani[4], Maximilian G. Schultz[4], Felix von Oppen[4] and Klaus Ensslin[1]

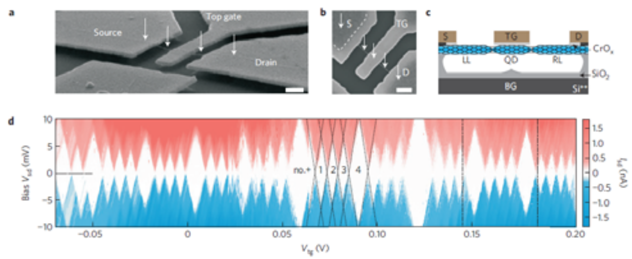

## Blokada Kulombowska

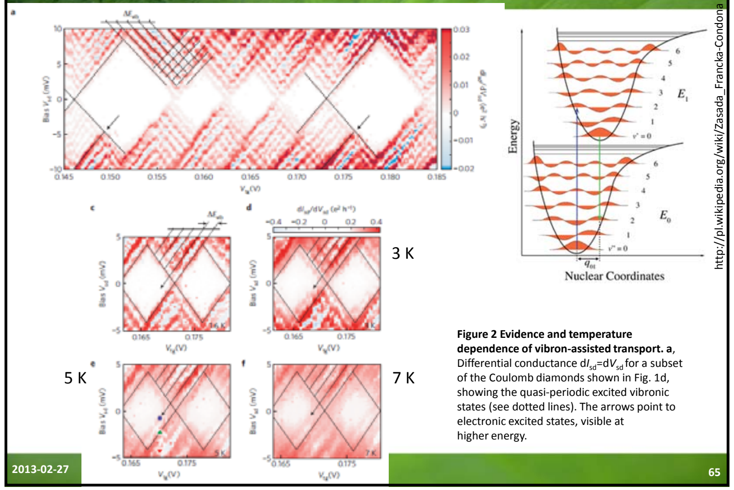


**Figure 2 Evidence and temperature dependence of vibron-assisted transport. a,** Differential conductance $dI_{sd}=dV_{sd}$ for a subset of the Coulomb diamonds shown in Fig. 1d, showing the quasi-periodic excited vibronic states (see dotted lines). The arrows point to electronic excited states, visible at higher energy.

2013-02-27 65

## Blokada Kulombowska

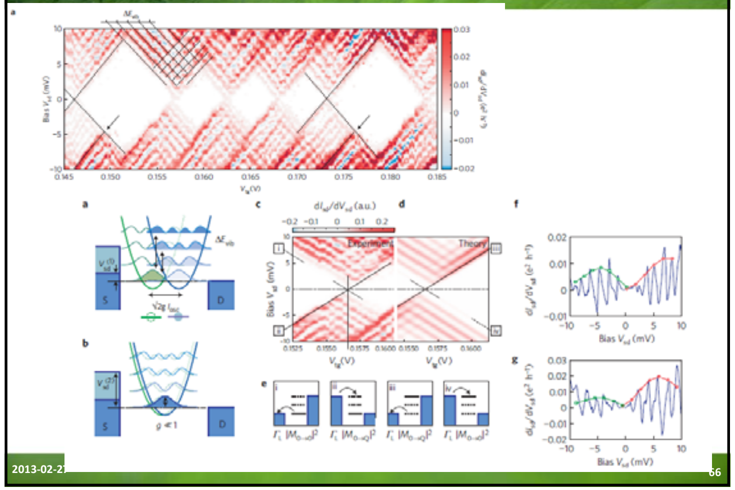


2013-02-27 66

## Pojedynczy odczyt pojedynczego spinu

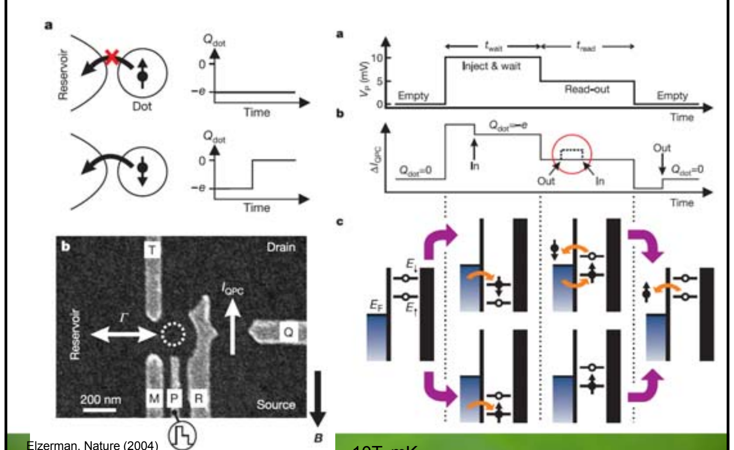


Elzerman, Nature (2004)

10T, mK

## Pojedynczy odczyt pojedynczego spinu

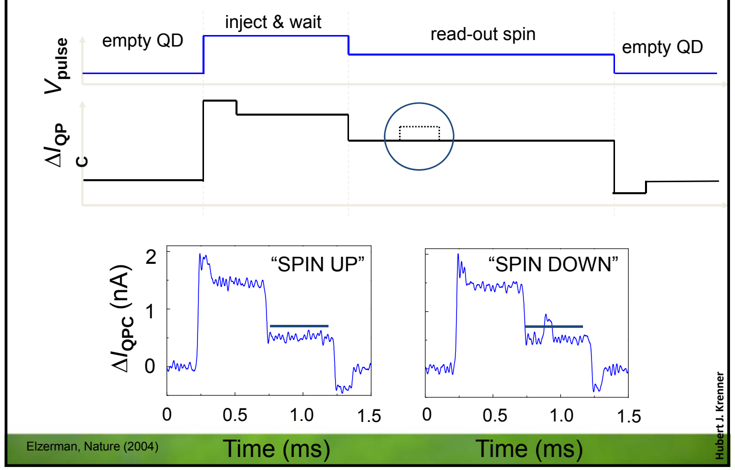


Elzerman, Nature (2004)

Hubert J. Krenner

## Spin storage

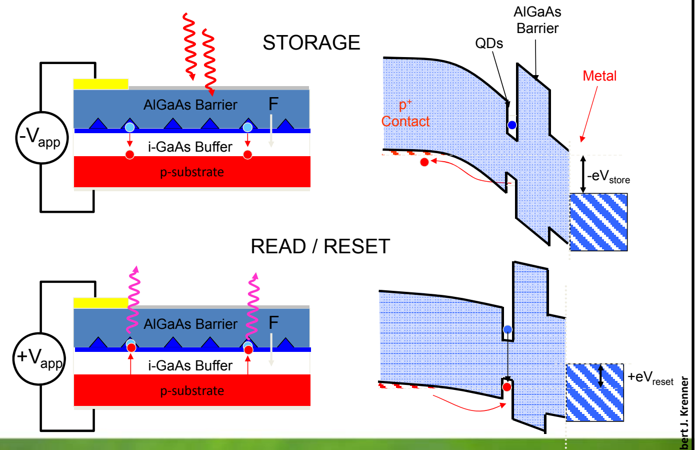


Kroutvar, Nature (2004)

## Blokada Kulombowska

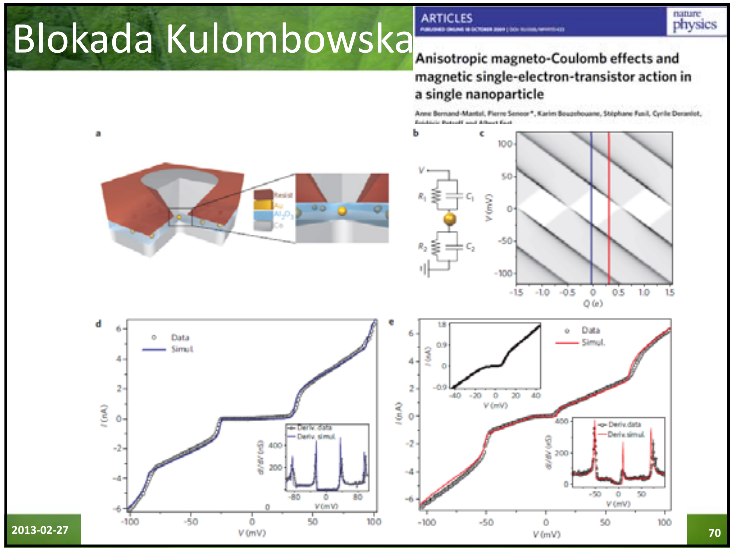




## Qubity

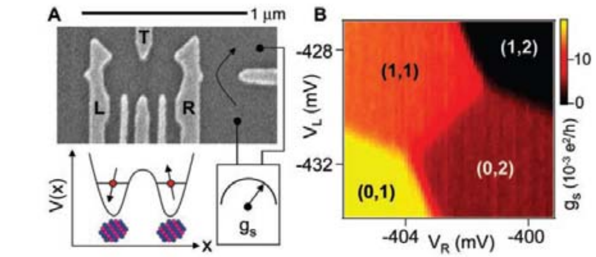


**Fig. 1.** (A) Scanning electron micrograph of a sample identical to the one measured, consisting of electrostatic gates on the surface of a two-dimensional electron gas. Voltages on gates L and R control the number of electrons in the left and right dots. Gate T is used to adjust the interdot tunnel coupling. The quantum point contact conductance $g_s$ is sensitive primarily to the number of electrons in the right dot. (B) $g_s$ measured as a function of $V_L$ and $V_R$ reflects the double-dot charge stability diagram (a background slope has been subtracted). Charge states are labeled (*m*,*n*), where *m* is the number of electrons in the left dot and *n* is the number of electrons in the right dot. Each charge state gives a distinct reading of $g_s$.

Coherent Manipulation of Coupled Electron Spins in Semiconductor Quantum Dots
J. R. Petta, et al. *Science 30 September 2005: 2180-2184.*



## Qubity

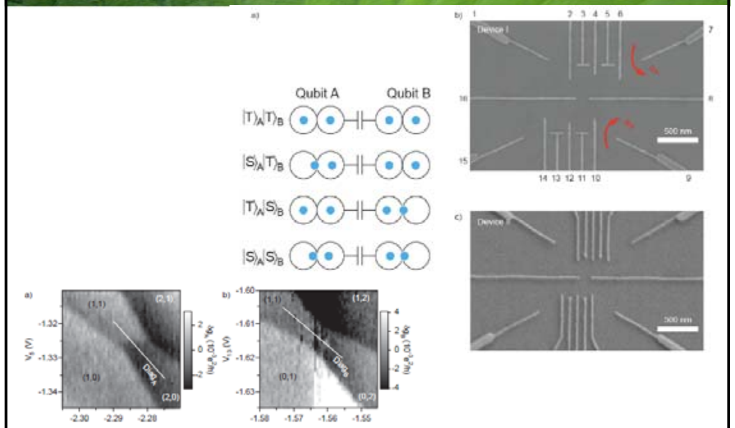


http://marcuslab.harvard.edu/theses/Laird_Thesis.pdf

# Qubity

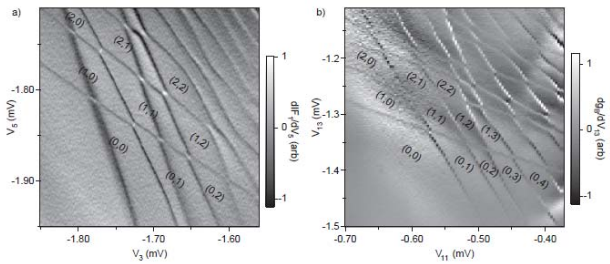


Figure 5.2: Charge stability diagrams of upper (a) and lower (b) double dots, measured using the charge sensors as a function of their respective plunger gate voltages. Both double dots can be tuned into the few-electron regime. The two broad near-vertical lines in (a) are resonances of the charge sensor.

http://marcuslab.harvard.edu/theses/Laird_Thesis.pdf